Journal of Materials Chemistry C

Accepted Manuscript

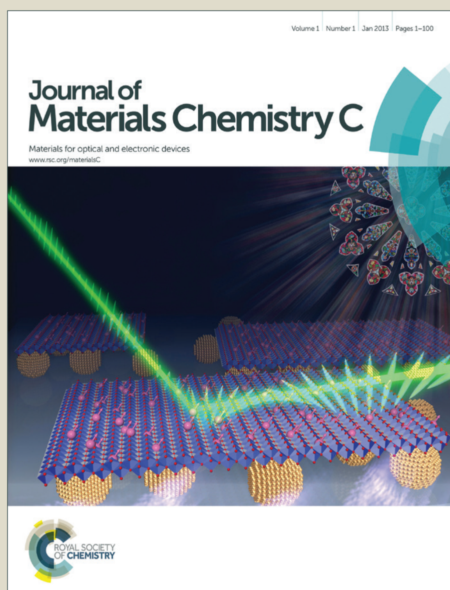

This is an *Accepted Manuscript*, which has been through the Royal Society of Chemistry peer review process and has been accepted for publication.

Accepted Manuscripts are published online shortly after acceptance, before technical editing, formatting and proof reading. Using this free service, authors can make their results available to the community, in citable form, before we publish the edited article. We will replace this *Accepted Manuscript* with the edited and formatted *Advance Article* as soon as it is available.

You can find more information about *Accepted Manuscripts* in the Information for Authors.

Please note that technical editing may introduce minor changes to the text and/or graphics, which may alter content. The journal's standard Terms & Conditions and the Ethical guidelines still apply. In no event shall the Royal Society of Chemistry be held responsible for any errors or omissions in this *Accepted Manuscript* or any consequences arising from the use of any information it contains.

ROYAL SOCIETY OF CHEMISTRY

www.rsc.org/materialsC

Role of vacancies to *p*-type semiconducting properties of SiGe nanowires

Rulong Zhou[1]*, Bingyan Qu[1], Bo Zhang[1], Pengfei Li[2], and Xiao Cheng Zeng[2,3]*

[1] *School of Science and Engineering of Materials, Hefei University of Technology, Hefei, Anhui 230009, P. R. China*

[2] *Department of Chemical Physics, University of Science and Technology of China, Hefei, Anhui 230026, P. R. China*

[3] *Department of Chemistry and Nebraska Center for Materials and Nanoscience, University of Nebraska-Lincoln, Lincoln, Nebraska 68588*

*rlzhou@hfut.edu.cn; *xzeng1@unl.edu

Abstract

Many experiments have shown that both composition-randomly-distributed $Si_{1-x}Ge_x$ nanowires (NWs) and the Ge-Si core-shell NWs possess excellent *p*-type semiconducting properties without relying on any doping strategy. Vacancies in both NWs are believed to play a key role for the *p*-type semiconducting properties. To gain deeper insights into the role of vacancies, we perform the first-principles calculations to systematically study effects of single Si or Ge vacancies in four distinct SiGe NWs, namely, randomly-distributed triangular-prism (RTP) NW, fused triangular-prism (FTP) NW, the $Ge_{core}Si_{shell}$ and $Si_{core}Ge_{shell}$ NWs. We find that tendency of vacancy formation depends strongly on structures of the NWs. The defective RTP, FTP and $Ge_{core}Si_{shell}$ NWs show promising *p*-type semiconducting properties while the defective $Si_{core}Ge_{shell}$ NW does not. The Si vacancies in the inner region are attributed to the *p*-type properties of the RTP NW, and both the Si and Ge vacancies at the core-shell interfaces are attributed to the *p*-type properties of the FTP and $Ge_{core}Si_{shell}$ NWs. Our results shed light on how the vacancies affect electronic structures and semiconducting properties of different SiGe NWs, and offer an explanation why the synthesized $Si_{1-x}Ge_x$ and $Ge_{core}Si_{shell}$ NWs possess excellent *p*-type semiconducting properties without relying on any doping strategy.

Journal of Materials Chemistry C Accepted Manuscript

Introduction

Semiconductor nanowires (NWs) are one of the most important one-dimensional (1D) nanostructures owing to their unique properties[1] and high potentials for applications in many fields such as field-effect transistors (FETs)[2,3], solar cells[4], integrated circuits[5], and biological or chemical sensors[6-11]. Among the 1D nanostructures, Si NWs are viewed as the most promising one for nanoelectronic devices due to the existing and mature Si-based semiconductor technology. However, previous experimental and theoretical studies have found that the semiconducting performance of Si NWs is not as good as Si bulk because it is more difficult to realize efficient electron- or hole-doping in Si NWs than in the bulk, implying that Si NWs may be not the best candidate nanostructures for nanoelectronic devices. Among others, one reason for the relatively low semiconducting performance of doped Si NWs is that ionization of the dopants in Si NWs is usually much harder than that in Si bulk due to the quantum confinement in Si NWs. To date, reducing the ionization energies of dopants in Si NWs is still an active area of research.

On the other hand, the search for other types of semiconductor nanostructures as alternatives to the Si NWs is also an active area of research in recent years. SiGe NWs have aroused extensive attention because of their novel electronic properties[12-25]. In fact, composition-randomly-distributed SiGe NWs (referred as $Si_{1-x}Ge_x$) have been successfully fabricated in the laboratory[16-21]. Importantly, the band gaps of $Si_{1-x}Ge_x$ NWs can be modulated over a wide range by tuning composition x and area of NW cross sections. Moreover, $Si_{1-x}Ge_x$ NWs possess *p*-type semiconducting properties without relying on any doping strategy, due possibly to the oxidation at the Si/Ge interfaces as elucidated in the literature. The $Ge_{core}Si_{shell}$ NWs have attracted even more attention in light of their high-density free hole gas revealed in the experiments (without implementation of any doping strategy), as well as recently established high-performance FETs based on $Ge_{core}Si_{shell}$ NWs[22-25].

Inspired by these previous experimental findings about SiGe core-shell NWs, much recent research efforts have been devoted to the origin of the high-density free

Journal of Materials Chemistry C Accepted Manuscript

hole gas in the $Ge_{core}Si_{shell}$ NWs, and how to realize efficient electron and hole doping in the NWs. The band offset at the radial heterojunction between the Ge core and Si shell, the Si dangling bonds at the surface, as well as metal impurities (transition metal particles are usually used as catalyst for the growth of SiGe NWs) were thought to be possible sources for contributing the high-density hole gas in the $Ge_{core}Si_{shell}$ NWs[26-28]. Amato *et al.* studied structure stabilities, electronic properties, quantum confinement effects of different types of SiGe NWs based on first-principles calculations[29-33]. They predicted that the $Ge_{core}Si_{shell}$ NWs are very stable energetically, and that efficient electron and hole doping can be easily realized due to the band offset in the type-II heterojunction of $Ge_{core}Si_{shell}$ NWs[34,35]. Following Amato's work, we have systematically studied substitution doping in various composition abrupt Si/Ge NWs using the first-principles method in view of the presence of type-II band offsets in other types of composition abrupt Si/Ge NWs in addition to the $Ge_{core}Si_{shell}$ NWs[36]. In our previous study, the core-shell Ge_{core}/Si_{shell} and Si_{core}/Ge_{shell} NWs, as well as the fused triangular-prism SiGe NW with much larger diameters were considered. The effects of dopants B, N, Al, P, or O were explored. Based on the first-principles calculations, substitution of Ge by the pentavalent P at the interfacial region of Ge/Si NWs results in an easy injection of high-density free-electron-like carriers, whereas substitution of Si by trivalent Al or B at the interfacial region results in an easy injection of high-density free-hole-like carriers. However, introduction of the pentavalent N has little effect on the conductivity of the three types of SiGe NWs. For the divalent O dopant, only substitution of Si by O in the fused triangular-prism SiGe NW can result in high-density free-hole-like carriers at low temperature. The efficient doping suggested from calculation was later realized by experiments in Ge_{core}/Si_{shell}[37] and Ge-Si_xGe_{1-x} core-shell NWs[38].

Note that in the fabricated $Si_{1-x}Ge_x$ NWs and Ge_{core}/Si_{shell} NWs, the *p*-type semiconducting characters are achieved without relying on any doping strategy. Although the oxidation at the interfaces and Au impurities are thought as possible reasons, vacancies at the interfaces may play even more important roles as vacancies are unavoidable in the growth of SiGe NWs. However, few studies have been reported

Journal of Materials Chemistry C Accepted Manuscript

on how different types of vacancies in different types of SiGe NWs can influence the electronic properties of SiGe NWs. To this end, we have studied effects of vacancies on the electronic properties of the following four types of SiGe NWs: (1) randomly-distributed triangular-prism (RTP) NW, (2) the fused triangular-prism (FTP) NW, (3) the $Ge_{core}Si_{shell}$ NWs, and (4) $Si_{core}Ge_{shell}$ NWs (see **Figure 1**).

Computational Details and Models of SiGe Nanowires

Our first-principles calculations are performed within the framework of density functional theory (DFT) as implemented in the *Siesta* 3.1 code[39]. We use norm-conserving pseudopotential for the core electrons and expand the one-electron wave-function of the valence electrons with a double-zeta basis set plus polarization functions. The Perdew-Burke-Ernzerhof (PBE)[40] exchange-correlation functional within the generalized gradient approximation (GGA) is employed. A real-space grid with an equivalent cutoff 180 Ry is adopted to expand the electron density for numerical integration. The periodic boundary condition is applied in all spatial directions, with the vacuum region among NWs >15 Å to neglect interaction among periodic images. For the randomly-distributed and fused triangular-prism NWs, three unit cells along the axial direction (lattice constants c are about 12.0 Å) are included in the supercell, which ensures that the interaction among the periodic images of the impurity can be neglected[41]. For the core-shell NWs, supercells containing two unit cells along the axial direction ($c \sim 8.0$ Å with which the interaction between periodic images is weak) are selected to reduce computational cost. For structural relaxation, 1×1×8 and 1×1×6 meshes within the Monkhorst-Pack special k-point scheme[42] in the Brillioun zone are considered for the core-shell and triangular-prism NWs, respectively. Denser k grids of 1×1×16 and 1×1×12 are used for the core-shell and triangular-prism NWs, respectively, in the calculation of electronic structures. Both mesh cutoff and the k points are tested carefully to make sure no significant changes in the total energy when their values are increased.

Journal of Materials Chemistry C Accepted Manuscript

All the SiGe NWs are oriented along the <110> direction (see **Figure 1**), i.e., the most common growth orientation for Si and Ge NWs[43]. The diameter of the core-shell and lateral length scale of the triangular-prism SiGe NWs are about 30 Å and 15 Å, respectively. For the core-shell NWs, the diameter of the core is about 10 Å. In the triangular-prism NWs, all the side surfaces are the {111} crystal planes which ensure high stability of the NW structures. For the core-shell NWs, a hexagon-like interface is selected to lower the computational cost. The dangling bonds on the surface are saturated with hydrogen atoms for all the NWs, which is an effective way to remove surface states within the band gap of the materials. The lattice constant along the growth orientation and the atomic positions of all the NWs are fully relaxed without symmetry constraints, using the conjugate-gradient algorithm. The geometric optimization is completed when the maximum component of the stress tensors and the maximum force on each atom are less than 0.5 GPa and 0.02 eV/ Å, respectively.

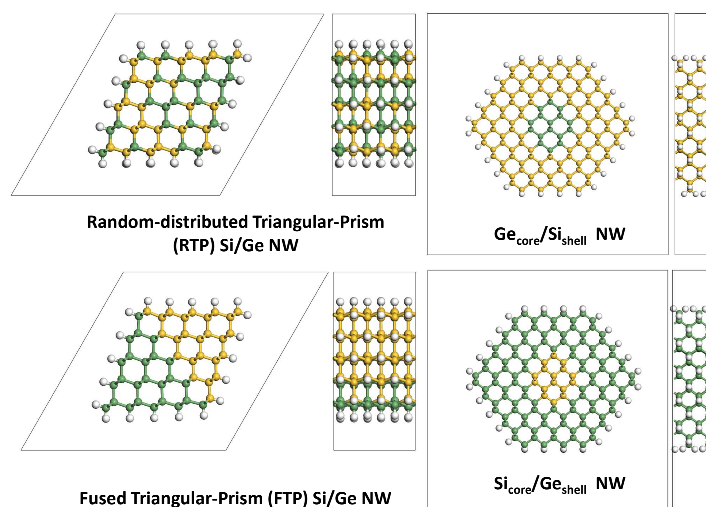

Figure 1 Model structures of Triangular-Prim (RTP) Si/Ge NW, Ge_{core}/Si_{shell} NW, Fused Triangular-Prism (FTP) Si/Ge NW, Random-distributed, and Si_{core}/Ge_{shell} NW, respectively. Color code: Si (gold), Ge (green), H (white).

Single atomic vacancies of Si and Ge at different sites in the Ge_{core}/Si_{shell}, Si_{core}/Ge_{shell}, fused triangular-prism (FTP) and randomly-distributed triangular-prism (RTP) Si/Ge NWs are considered. Positions of the vacancies are as shown in **Figure 2**.

Journal of Materials Chemistry C Accepted Manuscript

For the segregated Si/Ge NWs, i.e., Ge_{core}/Si_{shell}, Si_{core}/Ge_{shell}, and fused triangular-prism Si/Ge NWs, the vacancies near the interface between the Si and Ge parts are mainly considered, while for the randomly-distributed triangular-prism Si/Ge NWs, the Si (Ge) vacancies with different coordination surroundings are considered, *e.g.* vacancies of Si which are coordinated with four Ge atoms, three Ge and one Si, two Ge and two Si, one Ge and three Si, or four Si. For the Ge_{core}/Si_{shell} and Si_{core}/Ge_{shell} NWs, five different Si (Ge) vacancies, denoted as V_{Si1} to V_{Si5} (V_{Ge1} to V_{Ge5}), are studied. For the FTP Si/Ge NW, five Si (Ge) vacancies from the center to the surface of the NW, denoted as V_{Si1} to V_{Si5} (V_{Ge1} to V_{Ge5}), are investigated. The denotations of the vacancies are different for the RTP Si/Ge NW, where V_{Si0}, V_{Si1}, … , V_{Si4} represents the Si vacancies coordinated with zero, one, … , or four Ge atoms, while V_{Ge0}, V_{Ge1}, … , V_{Ge4} represents Ge vacancies coordinated with zero, one, … , or four Si atoms. According to our notation scheme, the cases of V_{Ge0} and V_{Si4} in the RTP NW have the same surrounding conditions, *i.e.* both are surrounded by four Ge atoms. Same conditions are true for V_{Ge1} and V_{Si3} , V_{Ge2} and V_{Si2} , V_{Ge3} and V_{Si1} , V_{Ge4} and V_{Si0}, respectively.

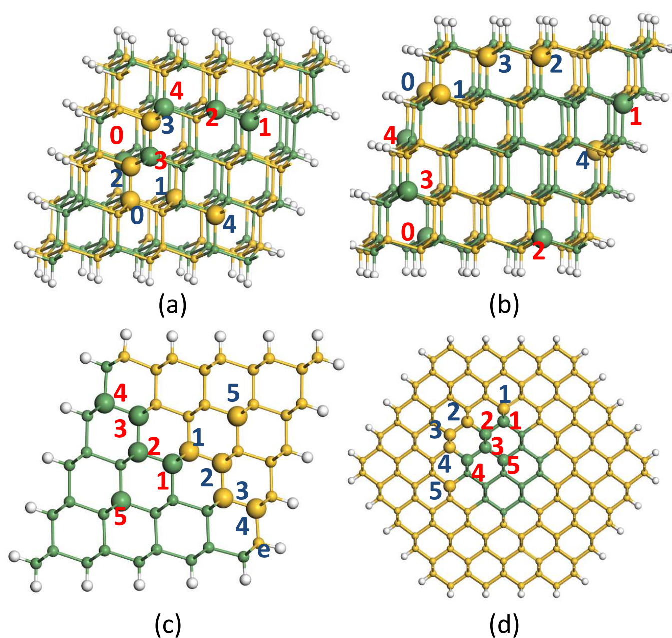

Figure 2 Positions of vacancies in (a) within the RTP Si/Ge NW (b) surface of the RTP Si/Ge NW (c) the FTP Si/Ge NW, and (d) the Ge_{core}/Si_{shell} NW. Positions of the vacancies of Ge are marked in

Journal of Materials Chemistry C Accepted Manuscript

red numbers, while those of Si are marked in blue numbers. Distribution of the vacancies in the Si_{core}/Ge_{shell} NW is similar to that in the Ge_{core}/Si_{shell} NW.

Results and Discussion

1. Relative stabilities of Ge and Si vacancies at different sites.

First, we evaluate relative possibilities of Ge an Si vacancy formation at different sites in the Si/Ge NWs by calculating the formation energies of vacancies based on the following formula

$$E_f = E_{tot} - E_{perfect} + \mu_{Si} \text{ (or } \mu_{Ge} \text{)}$$

where E_{tot} is the total energy of a Si/Ge NW containing one Si or Ge vacancy per supercell, $E_{perfect}$ is the total energy of the perfect Si/Ge NW, and μ_{Si}, μ_{Ge} are the chemical potentials of Si and Ge respectively. The calculated formation energies of Si and Ge vacancies at various sites considered in different Si/Ge NWs are listed in **Table I**.

Table I The formation energies of a single vacancy in different Si/Ge NWs. Lowest Si and Ge formation energies are highlighted in bold.

Vacancy Site	Formation Energy (eV)									
Body of	V_{Ge0}	V_{Ge1}	V_{Ge2}	V_{Ge3}	V_{Ge4}	V_{Si0}	V_{Si1}	V_{Si2}	V_{Si3}	V_{Si4}
RTP NW	**2.524**	2.792	2.834	3.313	2.971	3.029	2.497	2.773	2.584	**2.355**
Surface of	V_{Ge0}	V_{Ge1}	V_{Ge2}	V_{Ge3}	V_{Ge4}	V_{Si0}	V_{Si1}	V_{Si2}	V_{Si3}	V_{Si4}
RTP NW	**1.965**	2.158	2.439	2.484	2.951	2.555	2.592	2.691	**2.180**	2.451
FTP NW	V_{Ge1}	V_{Ge2}	V_{Ge3}	V_{Ge4}	V_{Ge5}	V_{Si1}	V_{Si2}	V_{Si3}	V_{Si4}	V_{Si5}
	3.137	2.205	2.206	**1.814**	2.594	3.061	3.385	2.580	**2.169**	3.784
Ge_{core}/Si_{shell}	V_{Ge1}	V_{Ge2}	V_{Ge3}	V_{Ge4}	V_{Ge5}	V_{Si1}	V_{Si2}	V_{Si3}	V_{Si4}	V_{Si5}
	2.482	2.089	1.899	2.100	**1.726**	2.372	1.919	1.948	**0.532**	3.051

Journal of Materials Chemistry C Accepted Manuscript

Si_{core}/Ge_{shell}	V_{Ge1}	V_{Ge2}	V_{Ge3}	V_{Ge4}	V_{Ge5}	V_{Si1}	V_{Si2}	V_{Si3}	V_{Si4}	V_{Si5}
	2.467	2.605	2.483	2.588	2.593	**2.412**	2.440	2.728	3.238	2.754

For all the Si/Ge NWs considered, the formation energies of Si or Ge vacancies are all positive (or endothermic). Thus, the higher the formation energy is, the harder it can be formed. The formation energies exhibit different trends for different types of NWs. For the RTP NW, the formation energies of Si vacancies tend to be a bit lower than those of Ge vacancies under the same surrounding condition within the body of the NW, namely, V_{Si1} *vs* V_{Ge3}, V_{Si2} *vs* V_{Ge2} , V_{Si3} *vs* V_{Ge1}, V_{Si4} *vs* V_{Ge0} , except V_{Si0} *vs* V_{Ge4}. However, the trend is reversed when the vacancies are on the surface. It is surprising that the formation of Si vacancy costs less energy than that of Ge under the same surrounding condition in the body of the RTF NW, even though the bonding strength of Si is usually stronger than that of Ge. A possible reason is that local structural relaxation around the Si vacancy is more substantial thereby results in more energy gain than that around the Ge vacancy when both are in the body. On the other hand, on the surface, local structural relaxation around either the Si or Ge vacancy is comparable in energy gain, so the effect of the bond strength due to losing an atom is more substantial. Obviously, the formation energies of Ge vacancies have an upward trend with increasing the number of surrounding Si atoms, while the trend of the formation energies of Si vacancies is downward with increasing the number of surrounding Ge atoms. These trend changes are entirely due to the stronger bonding of Si over Ge. The formation of vacancies on the surfaces is usually easier than that in the body because of higher freedom for the surrounding atoms of the vacancies on the surface than in the body.

For the FTP NW, the formation energies of Si vacancies tend to be a bit higher than those of Ge vacancies at similar sites, again due to the stronger bonding of Si over Ge. When the vacancies are located on the surface, the formation energies tend to decrease. As shown in **Table I**, the formation energies of Ge and Si vacancies in the FTP NW are slightly lower than those at the similar places (referring to **Figure 2**) in

Journal of Materials Chemistry C Accepted Manuscript

the RTP NW. So, vacancies are easier to be generated near the flat interface.

For the core-shell NWs, it seems more difficult to generate a vacancy in the core than in the shell as shown in **Table I**, contrary to the trend for the substituted dopants for which the substitution in the core is slightly preferred over the shell[36]. Among the four types of Si/Ge NWs, formation of vacancies in the Ge_{core}/Si_{shell} NW seems the easiest. The lowest formation energies of Ge and Si vacancies near the interface of the Ge_{core}/Si_{shell} NW are 1.726 and 0.532 eV, respectively (see **Table I**). It should be noted that the Ge_{core}/Si_{shell} NW is also the most stable type of Si/Ge NW according to previous calculations[31-33]. Hence, we expect that in the realistic Ge_{core}/Si_{shell} NWs more vacancies would be formed at the core/shell interfaces. This is possibly a main reason for the high density of hole gas detected in the Ge_{core}/Si_{shell} NWs [22-25].

2. Electronic structures

a) Vacancies in the random-distributed triangular-prism (RTP) Si/Ge NWs

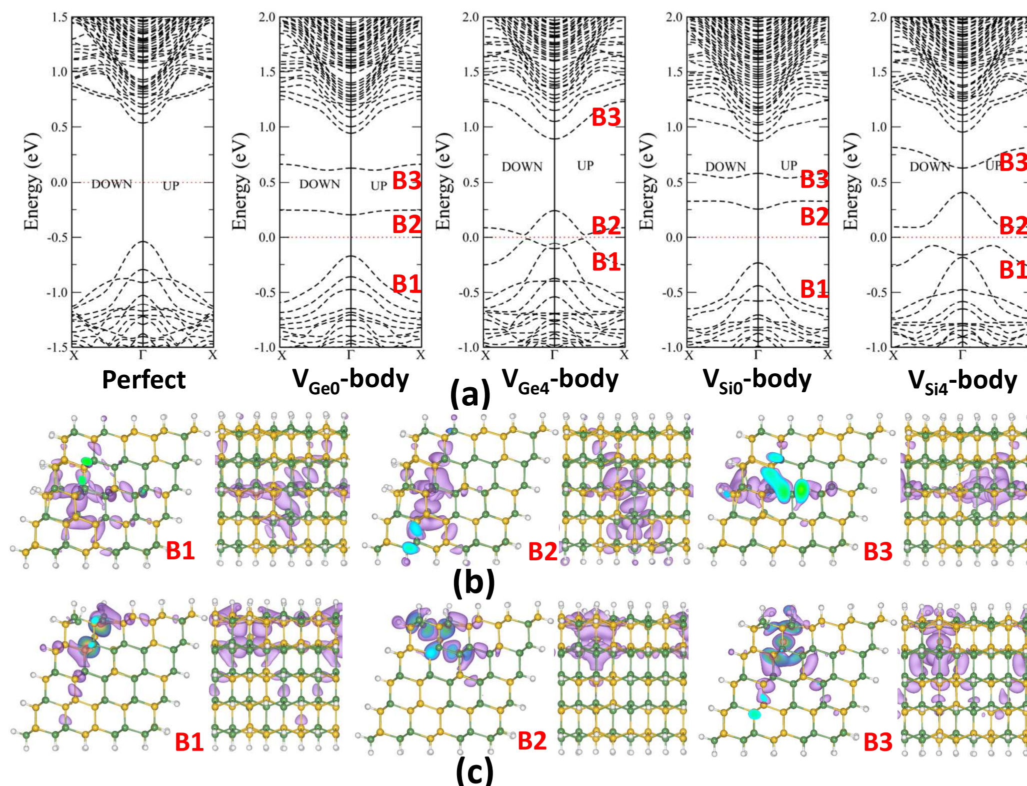

Figure 3 (a) Computed band structures of the random-distributed triangular-prism (RTP) Si/Ge

Journal of Materials Chemistry C Accepted Manuscript

NWs with a Ge and Si single vacancy in the body. Wave-function iso-surface of the defect bands near the Fermi level for (b) the V_{Ge0}-body, and (c) the V_{Ge4}-body. The iso-surface value is 0.05.

First, we consider the vacancies in the body of the RTP Si/Ge NWs. Although the surroundings of vacancies are different, the computed electronic structures are quite similar. We select two Ge vacancies and two Si vacancies for discussion. Computed band structures along with those of the perfect RTP Si/Ge NW, are shown in **Figure 3**. The band structures for other vacancy systems are shown in the Electronic Supplementary Information (ESI) Figure S1[†]. For V_{Ge0}-body system, two flat bands (B2,B3) originated from the vacancies are located within the band gap. The two flat bands cannot lead to carrier conduction, as indicated by the wave-function iso-surface (see **Figure 3** (b)). The wave-functions corresponding to B2 and B3 bands are apparently localized at the vacancy area, and they do not extend to the whole supercell along the axial direction. Besides the two non-conduction bands, there is a conduction band below the Fermi level, originated mainly from the states of the defect (B1 band). It lies above the top of the valance bands and tilts downward. So it can lead to hole conduction. From the band structures, we know that V_{Ge0}-body in the RTP Si/Ge NW acts as both defective center and acceptor. The roles of V_{Ge1}-body, V_{Ge2}-body and V_{Ge3}-body are similar as V_{Ge0}-body, and their corresponding band structures (see ESI Figure S1) are close to those of V_{Ge0}-body system too. For V_{Ge4}-body system, the band structures are much different from those of V_{Ge0}-body to V_{Ge3}-body systems. The three defect bands all exhibit curvatures. B1 tilts downward similar to that of V_{Ge0}-body, while B2 and B3 tilt upward. So, B1 is a valance band while B2 and B3 are conduction bands. Comparing to the band structures of V_{Ge0}-body system, the bands B2 and B3 of V_{Ge4}-body system depart from one another so that B2 moves below the top of B1 band and cross with it. Due to the repulsion between B1 and B2 bands, a very small gap opens at the crossing point of the B1 and B2 bands. The Fermi level is just located in this small gap. Hence, holes can be easily generated. We expect that in this case high density hole gas may exist at finite temperatures.

Journal of Materials Chemistry C Accepted Manuscript

For the Si vacancy, the band structures of V_{Si0}-body system are very similar to those of V_{Ge0}-body system. Near the energy gap, there are two localized bands (B2, B3) and one delocalized band (B1) originated from the Si vacancy. The band structures of V_{Si4}-body system are similar to those of V_{Ge4}-body system. An obvious difference between the band structures of V_{Si4}-body and V_{Ge4}-body is that the gap between B1 and B2 for V_{Si4}-body system is a bit larger than that of V_{Ge4}-body system. So, generation of carriers would be a bit harder with the Si vacancies. The band structures of V_{Si1}-body to V_{Si3}-body systems are all similar to those of V_{Si4}-body system (see ESI Figure S1).

Interestingly, the band structures of V_{Ge0} and V_{Si4}, and those of V_{Ge4} and V_{Si0} are quite different while the vacancy surroundings in these systems are the same (four Ge atoms for V_{Ge0} and V_{Si4}, four Si atoms for V_{Si0} and V_{Ge4}, respectively). The local structure relaxation at the vacancy sites may be the main reason for this difference. So the electronic properties of the compositionally-random-distribution SiGe NWs can be hard to predict. Relative formation abilities of different vacancies may give some guidance about their electronic properties. Referring to **Table I**, since the formation energy of V_{Ge0}-body is the lowest while that of V_{Ge4}-body is the highest, V_{Ge0}-body vacancies have a higher possibility to be generated. On the other hand, for Si vacancies, generation of V_{Si4}-body vacancies has the highest possibility while that of V_{Si0}-body vacancies is hardest. So, in the RTF NW, if the vacancies are mainly Ge vacancies, the NW should be insulating, while if the vacancies are mainly Si vacancies, the NW would be semiconducting. Generation of the V_{Si4}-body vacancies is slightly easier than V_{Ge0}-body vacancies, so the defective RTF NW is more likely to be semiconducting if the vacancies are located in the body of the NW.

Journal of Materials Chemistry C Accepted Manuscript

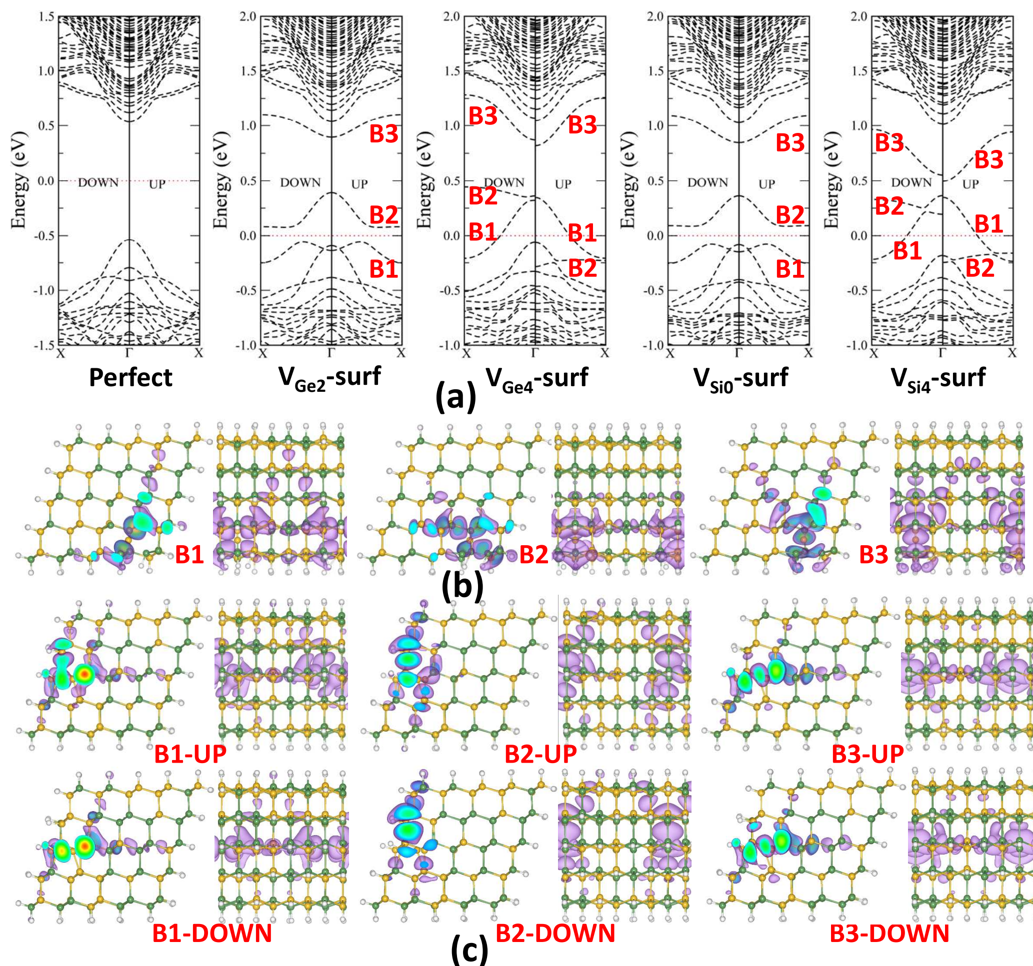

Figure 4 (a) Computed band structures of the random-distributed triangular-prism (RTP) Si/Ge NWs with a Ge and Si single vacancy on the surface. Wave-function iso-surface of the defect bands near the Fermi level for (b) the V_{Ge2}-surf, and (c) the V_{Ge4}-surf systems. The iso-surface value is 0.05.

Next, we study how the vacancies on the surfaces of the random-distributed triangular-prism (RTP) NWs influence their electronic structures. The band structures of V_{Ge2}-surf and V_{Ge4}-surf systems, as well as V_{Si0}-surf and V_{Si4}-surf systems are shown in **Figure 4**. The band structures of other systems are shown in ESI Figure S2. From the band structures, one can see that V_{Ge0}-surf, V_{Ge1}-surf, V_{Ge3}-surf and V_{Si3}-surf systems cannot conduct current at low temperatures because the defective bands are strongly localized as in the V_{Ge0}-body system. The band structures of

Journal of Materials Chemistry C Accepted Manuscript

V_{Ge2}-surf, V_{Si0}-surf, V_{Si1}-surf and V_{Si2}-surf systems are similar, as those of V_{Ge4}-body. The B1 and B2 bands cross one another and also repel each other, resulting in a small band gap (about 0.2 eV in these cases). The Fermi level is just located within the small band gap, implying that holes can be generated at finite temperatures. In summary, all these vacancy systems show *p*-type semiconducting properties.

We also notice a very different and interesting behavior in the band structures of V_{Ge4}-surf and V_{Si4}-surf systems. As shown in **Figure 4**, the Fermi level crosses the B1 band for both systems. Because the B1 band suggests good conduction due to the extensively delocalized distribution of the wave-functions along the axial direction, V_{Ge4}-surf and V_{Si4}-surf NWs are predicted to be conductors. Moreover, the spin polarized B2 band splits remarkably. The spin-down band moves up relatively. Different from the V_{Ge2}-surf and V_{Si0}-surf systems, there is no gap opening between bands B1 and B2 for the V_{Ge4}-surf and V_{Si4}-surf systems. The reason for the spin splitting may be the strong repulsion between the conduction band B1 and the non-conduction band B2. Interestingly, the spin splitting only occurs in the V_{Ge4}-surf and V_{Si4}-surf systems, in which the vacancy sites are surrounded by four Si atoms or four Ge atoms, and this only occurs for the highly localized B2 bands.

Note also that the formation energies of V_{Ge0}-surf and V_{Ge1}-surf vacancies are obviously lower than those of other Ge vacancies, and the formation energy of V_{Si3}-surf is obviously lower than those of other Si vacancies. For V_{Ge0}-surf, V_{Ge1}-surf, and V_{Si3}-surf systems, computed band structures show that they are all insulators. Thus, the vacancies on the surface of a RTF NW give no help to conductivity of the NW.

In Ref. 21, Seong *et al*. reported that the synthesized Si_xGe_{1-x} NWs exhibit *p*-type feature and they attributed this feature to the oxidation of Ge at the interfaces between Si_xGe_{1-x} and SiO_x oxidation surfaces. According to our calculations, the point vacancy defect may be another reason for their *p*-type semiconducting properties. The contribution of the vacancies to the *p*-type semiconducting properties was not considered in Ref. 21 because the density of vacancies is much lower compared to that of oxidation. For an oxidation-free Si_xGe_{1-x} NW, the vacancies can lead to *p*-type

Journal of Materials Chemistry C Accepted Manuscript

semiconducting properties.

b) Vacancies in the fused-triangular-prism (FTP) Si/Ge NWs

For the fused-triangular-prism Si/Ge NW, there is an abrupt interface between Si and Ge sections. We consider four different Si vacancies (V_{Si1} to V_{Si4}) and four Ge vacancies (V_{Ge1} to V_{Ge4}) at the interface, respectively. For comparison, the Si vacancy and Ge vacancy at the center of Si portion and Ge portion (V_{Si5} and V_{Ge5}) are also considered. Computed band structures of all systems as well as those of the perfect FTP Si/Ge NW are shown in **Figure 5**. The computed band structures of V_{Ge3} system are very similar to those of V_{Ge2} system.

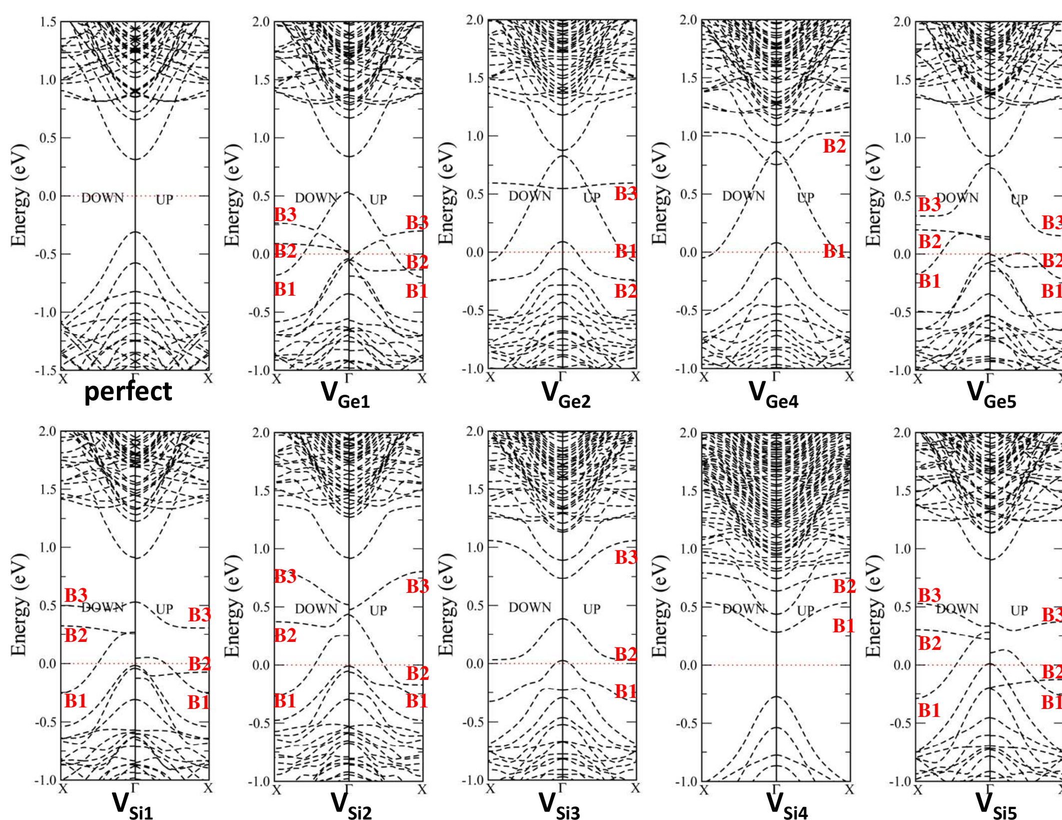

Figure 5 Computed band structures of the fused-triangular-prism (RTP) Si/Ge NWs with Ge and Si single vacancy at various sites.

As seen in **Figure 5**, in most systems, the vacancies in the FTP Si/Ge NW

Journal of Materials Chemistry C Accepted Manuscript

introduce three defect bands within the band gap of the perfect FTP/SiGe NW. The electronic properties of each defect band can be understood from their wave-function distributions. In **Figure 6**, the wave-function iso-surfaces corresponding to the defect bands of V_{Ge1}, V_{Ge4}, V_{Si1} and V_{Si4} systems are shown. Apparently, in all systems, B1 bands correspond to the conduction bands as the band lines disperse over extensive energy ranges and the associated wave functions are delocalized along the axial direction. Furthermore, for most systems the B1 band should lead to hole conduction because their band lines tilt downward from the center of the first Brillouin zone to the surface (Γ to X), except those of V_{Si4} system. The B2 bands for all systems are normally very flat and localized. As shown in, the wave-functions of B2 band distribute dispersedly along the interface, but are localized along the axial direction. So, the B2 bands for all systems cannot lead to carrier conduction. The wave-functions of B3 bands are also mainly localized around the vacancy sites, and exhibit little delocalization along the axial direction in some systems. So, the B3 bands may give minor conduction of holes or electrons.

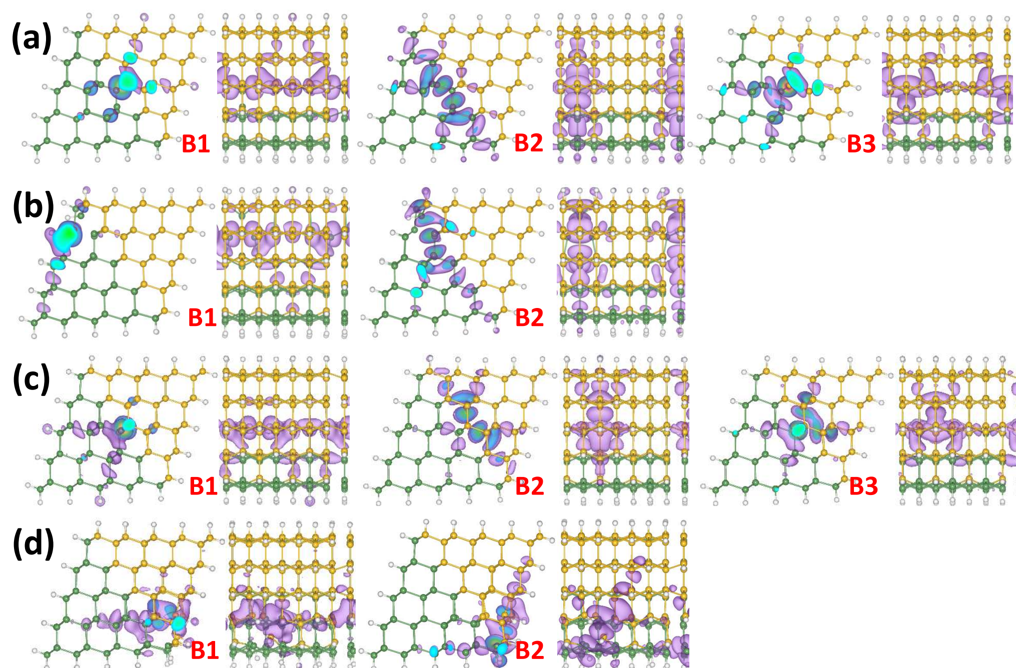

Figure 6 Computed wave-function isosurface corresponding to the defect bands for the (a)V_{Ge1} (b) V_{Ge4} (c) V_{Si1} and (d) V_{Si4} vacancy, respectively, in the fused-triangular-prism Si/Ge NW. The

Journal of Materials Chemistry C Accepted Manuscript

isosurface value is 0.05.

In addition, spin splitting is seen for the V_{Ge1}, V_{Ge5}, V_{Si1}, V_{Si2} and V_{Si5} systems but not others. Again, the spin splitting mainly occurs in the highly delocalized B2 bands. For some systems, the B3 bands exhibit spin splitting too. The Fermi levels for these five systems all cross the corresponding conduction B1 bands. For the V_{Ge2}, V_{Ge3} and V_{Ge4} systems, **Figure 5** clearly shows that the Fermi levels cross both the top valance band and the B1 defect band, resulting in carrier conduction. The B2 and B3 bands for V_{Ge4} system are very high compared to those for other Ge vacancy systems. The B3 band (not marked in **Figure 5**) even merges to the conduction bands for V_{Ge4} system. For V_{Si3} system, the maximum of the valance band and the minimum of the B1 band are almost the same. The Fermi level is just located above the maximum of the valance band. So, V_{Si3} system may also have good conductivity.

Again, V_{Si4} system is quite different. As shown in **Figure 5**, the B1 band for V_{Si4} system is close to the conduction bands and tiles upwards, suggesting good conductivity due to electrons but not holes. Both B1 and B2 bands are located very high, far from the top valance band. A relatively big band gap (~0.5 eV) is seen between the top valance band and the B1 band, and the Fermi level is located at the center of the gap. Contrary to other systems, V_{Si4} system is an insulator at low temperatures. As shown in **Figure 6**(d), the wave-functions of B2 band for V_{Si4} system are mainly contributed by the vacancy states and the surface states, but not the interface states.

In summary, with vacancies in the FTP Si/Ge NW, except V_{Si4} system, all systems are semiconducting. Because the formation of Ge vacancies is easier than that of Si vacancies in the FTP Si/Ge NW, the defective FTP Si/Ge NWs likely have high possibility to exhibit *p*-type semiconducting properties.

c) Vacancies in the Ge_{core}/Si_{shell} NWs and Si_{core}/Ge_{shell} NWs

The Ge_{core}/Si_{shell} NWs are important because of their high hole conductivities demonstrated from experiments. The vacancies, especially those at the interface areas,

Journal of Materials Chemistry C Accepted Manuscript

may be attributed to the high conductivities for the undoped Ge_{core}/Si_{shell} NWs. Here, we consider various Si or Ge vacancies near the interfaces of the Ge_{core}/Si_{shell} NWs. Computed band structures for V_{Ge1} to V_{Ge5} and V_{Si1} to V_{Si4} systems, as well as those of the perfect Ge_{core}/Si_{shell} NW, are shown in **Figure 7**. The band structures of V_{Si5} system are almost the same as those of V_{Si4} system although their stabilities are much different.

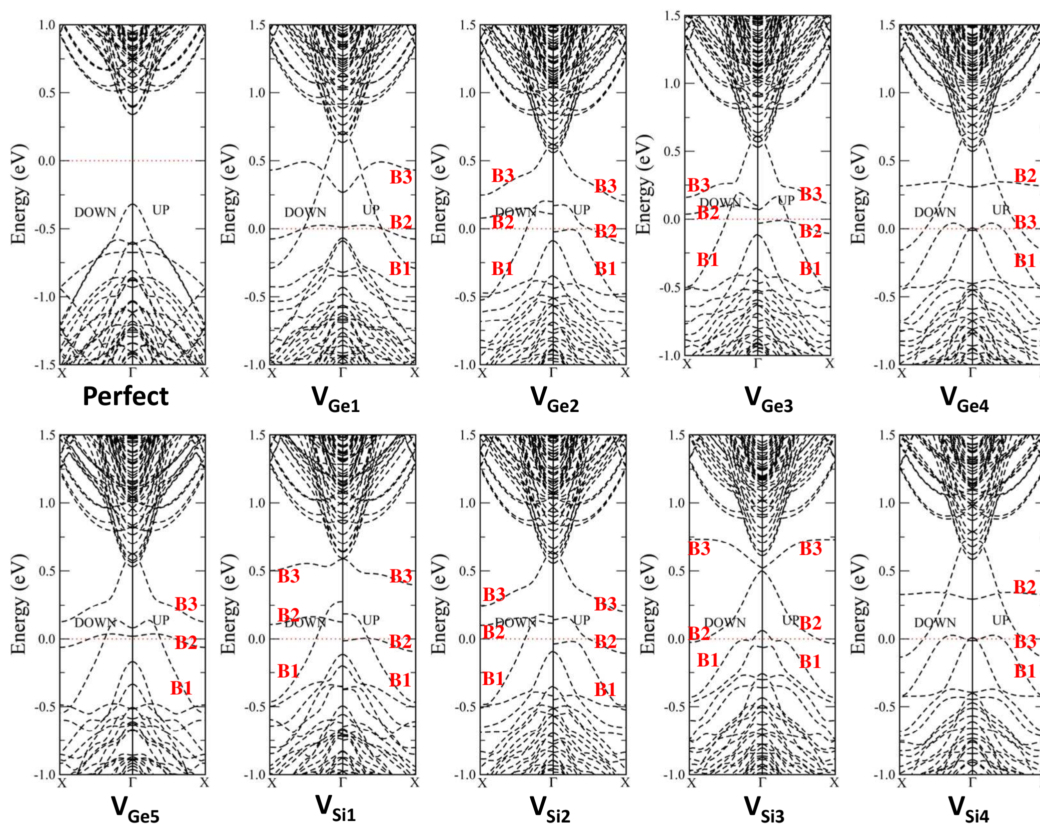

Figure 7 Computed band structures of the Ge_{core}/Si_{shell} NWs with Ge and Si single vacancy at various sites in the intersection area.

Journal of Materials Chemistry C Accepted Manuscript

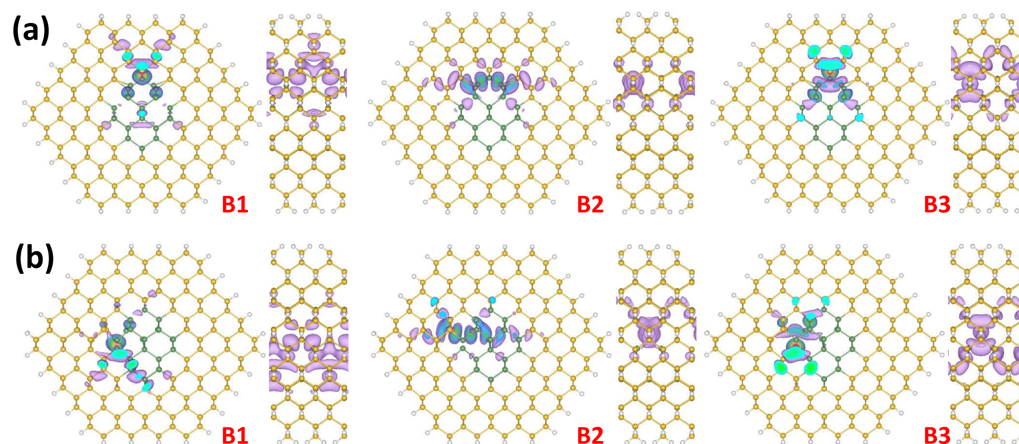

Figure 8 Computed wave-function iso-surface of the defect bands for (a) V_{Ge1} (b) V_{Ge4} vacancy in the Ge_{core}/Si_{shell} NW. The iso-surface value is 0.05

Compared to the band structures of the perfect Ge_{core}/Si_{shell} NW, one can easily see that the defects result in three bands in the gap region, named as B1, B2, and B3 bands according to their wave-function distributions (**Figure 8**). B1 band is a highly delocalized. It disperses over the band gap for the Ge_{core}/Si_{shell} NW. So, it is a conduction band. Because it tilts downward along the direction $\Gamma \rightarrow$ X, the conducting carriers should be holes. The B2 band is flattest among the three defect bands. It is also localized and cannot lead to carrier conduction. The wave-functions of B2 band are localized along the axial direction and slightly delocalized along the radial directions. The wave-function distribution of B3 band is between those of B1 and B2 bands. In some cases, it is quite flat while in other cases it is not. Normally, the B3 band tilts upward firstly then turns downward, along the direction $\Gamma \rightarrow$ X in the Brillouin Zone. Due to the high localization, in some systems, the spin polarized B2 and B3 bands are split.

For all systems, the Fermi levels cross at least the B1 band. Because the B1 band suggests high conductivity for holes, all systems should have good conductivities. In experiments, high density of hole carriers are found in the core of the Ge_{core}/Si_{shell} NWs[22-25]. Park *et al.*[28] studied the Si dangling bond on the surface and the Au impurity within the Si shell of the Ge_{core}/Si_{shell} NWs to explain why a high density of holes is present in the Ge_{core}/Si_{shell} NWs. However, the dangling bonds at the

Journal of Materials Chemistry C Accepted Manuscript

interfaces were not considered. Vacancies are expected to be formed more easily at the interfaces than in the inner part of core or shell during the growth, due to the mismatch of the lattice constants and the constraint stresses. The hole carriers generated due to the ionization of the vacancies at the interfaces are easier to transfer to the core region, compared to those generated on the surfaces. Therefore, the vacancies at the interfacial region of the Ge_{core}/Si_{shell} NW are more likely to give rise to a high-density hole gas as demonstrated in experiments.

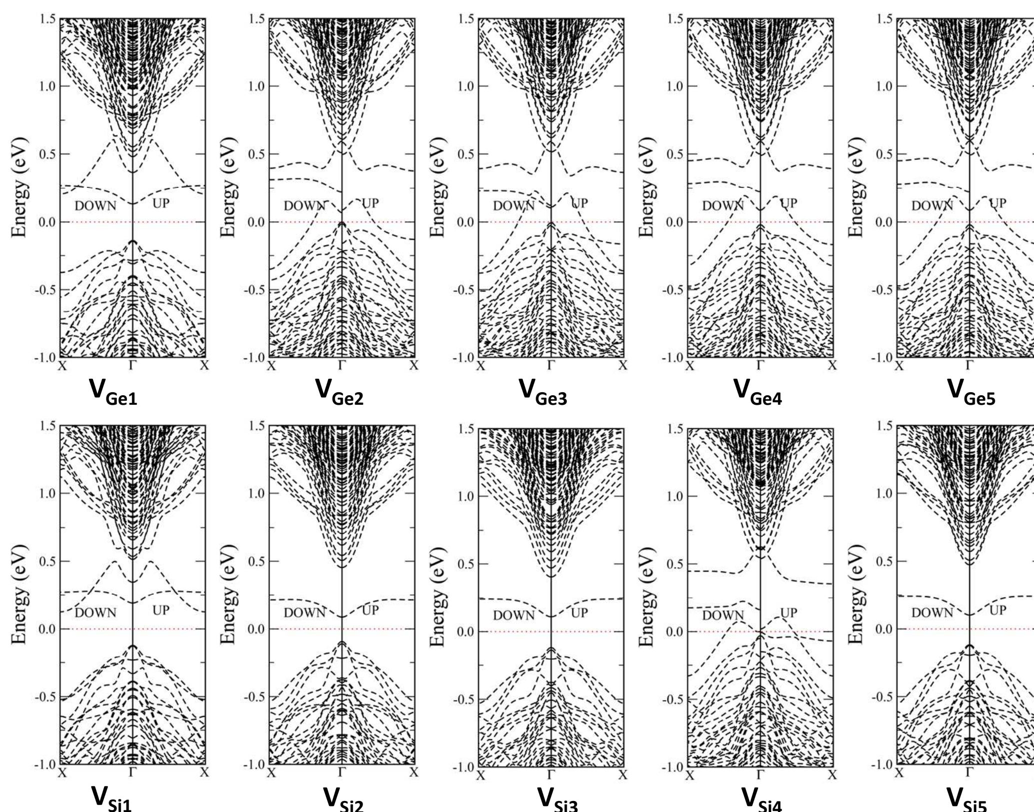

Figure 9 Computed band structures of the Si_{core}/Ge_{shell} NWs with Ge and Si single vacancy at various sites in the intersection area.

For the Si_{core}/Ge_{shell} NW, the difference in stress at the interface region makes the band structures of Si_{core}/Ge_{shell} NW much different from those of the Ge_{core}/Si_{shell} NW (see **Figure 9**). Apparently, with the Ge vacancies, most systems are still conducting, except the V_{Ge1} system. However, with the Si vacancies, all systems are not

Journal of Materials Chemistry C Accepted Manuscript

conducting due to the lack of band crossing through the Fermi level. By comparing the band structures of the Si_{core}/Ge_{shell} NW and the Ge_{core}/Si_{shell} NW, one can see that for the non-conducting systems, the B1 band is either shifted upward, leaving a big gap from the Fermi level, or downward into the valence bands. For the conducting systems, V_{Ge2} to V_{Ge5} and V_{Si4}, the formation energies of vacancies are all much higher than those for the Ge_{core}/Si_{shell} NW. So vacancies in the Si_{core}/Ge_{shell} NW are not as important contribution as those in the Ge_{core}/Si_{shell} NW to the conductivity.

Conclusion

We have studied effects of single vacancies on semiconducting properties of four different types of SiGe NWs, i.e., randomly-distributed triangular-prism (RTP) NW, the fused triangular-prism (FTP) NW, the $Ge_{core}Si_{shell}$ and $Si_{core}Ge_{shell}$ NWs. Si and Ge vacancies at different sites are investigated. Calculated formation energies indicate that the formation tendency of single Si or Ge vacancies is strongly dependent on the structures of the NWs. The formation of vacancies at the interface of the $Ge_{core}Si_{shell}$ NW entails least energy among all the NWs considered. The computed band structures suggest that the defective RTP, FPT and $Ge_{core}Si_{shell}$ NWs exhibit *p*-typing semiconducting properties, while the semiconducting properties of the defective $Ge_{core}Si_{shell}$ NW are much less apparent. For the RTP NW, the hole-carriers are likely originated from the Si vacancies located in the inner area, while in the FPT and $Ge_{core}Si_{shell}$ NWs both Si and Ge vacancies at the interfaces can generate high-density hole carriers. The hole injection in the $Ge_{core}Si_{shell}$ NW is likely the easiest among all the NWs considered. Our theoretical results are consistent with the experimental observations, thereby providing a compiling explanation on why the experimentally synthesized $Si_{1-x}Ge_x$ and $Ge_{core}Si_{shell}$ NWs can exhibit remarkable *p*-type semiconducting properties without relying on any doping strategy.

Journal of Materials Chemistry C Accepted Manuscript

Acknowledgements: This work is supported by the National Natural Science Foundation of China (Grant No. 11104056), the Natural Science Foundation of Anhui Province (Grant No. 11040606Q33). XCZ is supported by ARL (Grant No. W911NF1020099) and a grant from USTC for (1000 Talents Plan) Qianren-B summer research.

†Electronic supplementary information (ESI) available: Computed band structures of the random-distributed triangular-prism (RTP) Si/Ge NWs with Ge and Si single vacancy in the body and on the surface.

References

1. D. D. D. Ma, C. C. Lee, F. C. K. Au, S. Y. Tong, S. T. Lee, *Science*, 2003, **299**, 1874-1877.
2. Y. Cui, and C. M. Lieber, *Science*, 2001, **291**, 851-853.
3. J. Xiang, W. Lu, Y. J. Hu, Y. Wu, H. Yan, and C. M. Lieber, *Nature,* 2006, **441**, 489-493.
4. T. J. Kempa, B. Z. Tian, D. R. Kim, J. S. Hu, X. L. Zeng, and C. M. Lieber, *Nano Lett.,* 2008, **8**, 3456-3460.
5. S. W. Nam, X. C. Jiang, Q. H. Xiong, D. Ham, and C. M. Lieber, *Proc. Natl. Acad. Sci. USA*, 2009, **106**, 21035-21038.
6. Y. Cui, Q. Q. Wei, H. K. Park, and C. M. Lieber, *Science*, 2001, **293**, 1289-1292.
7. P. Alivisatos, *Nature Biotechnology*, 2004, **22**, 47-52.
8. G. F. Zheng, F. Patolsky, Y. Cui, W. U. Wang, and C. M. Lieber, *Nature Biotechnology,* 2005, **23**, 1294-1301.
9. J. Hahm, C. M. Lieber, *Nano Lett.,* 2004**, 4**, 51-54.
10. F. Patolsky, G. F. Zheng, O. Hayden, M. Lakadamyali, X. W. Zhuang, and C. M. Lieber, *Proc. Natl. Acad. Sci.USA,* 2004, **101**, 14017-14022.

Journal of Materials Chemistry C Accepted Manuscript

11. W. U. Wang, C. Chen, K.-H Lin, Y. Fang, C. M. Lieber, *Proc. Natl. Acad. Sci. USA*, 2005, **102**, 3208-3212.
12. M. Amato, M. Palummo, R. Rurali, and S. Ossicini, *Chem. Rev.* 2014, **114**, 1371-1412.
13. M. Amato, S. Ossicini, and R. Rurali, *Nano Lett*. 2012, **12**, 2717-2721.
14. L. Zhang, M. d'Avezac, J.-W. Luo, and A. Zunger, *Nano Lett*. 2012, **12**, 984-991.
15. T. Markussen, *Nano Lett*. 2012, **12**, 4698-4704.
16. J. E. Yang, C. B. Jin, C. J. Kim, and M. H. Jo, *Nano Lett*. 2006, **6**, 2679-2684.
17. X. Zhang, K.-K. Lew, P. Nimmatoori, J. M. Redwing, and E. C. Dickey, *Nano Lett.* 2007, **7,** 3241-3245.
18. C. Qi, G. Goncher, R. Solanki and J. Jordan, *Nanotechnology*, 2007, **18**, 075302
19. U. Givan and F. Patolsky, *Nano Lett*. 2009, **9**, 1775-1779.
20. T. Shimizu, Z. Zhang, S. Shingubara, S. Senz, and U. Gösele, *Nano Lett*. 2009, **9**, 1523-1526.
21. H. K. Seong, E. K. Jeon, M. H. Kim, H. Oh, J. O. Lee, J. J. Kim, and H. J. Choi, *Nano Lett*. 2008, **8,** 3656-3661.
22. J. Xiang, W. Lu, Y. J. Hu, Y. Wu, H. Yan and C. M Lieber, *Nature*, 2006, **441**, 489-493.
23. W. Lu, J. Xiang, B. P. Timko, Y. Wu, C. M. and Lieber, *Proc. Natl. Acad. Sci. USA*, 2005, **102**, 10046-10051.
24. S. X. Zhang, F. J. Lopez, J. K. Hyun, and L. J. Lauhon, *Nano Lett.*, 2010, **10**, 4483-4487.
25. L. Y. Li, D. J. Smith, E. Dailey, P. Madras, J. Drucker, and M. R. McCartney, *Nano Lett*, 2011, **11**, 493-497.
26. L. Yang, R. N. Musin, X. Q. Wang, and M. Y. Chou, *Phys. Rev. B*, 2008, **77**, 195325(1-5).
27. A. Nduwimana, R. N. Musin, A. M. Smith, X. Q. Wang, *Nano Lett*, 2008, **8**, 3341-3344.
28. J. S. Park, B. Ryu, C. Y. Moon, K. J. Chang, *Nano Lett*, 2010, **10**, 116-121.
29. M. Amato, M. Palummo, S. Ossicini, *Mat. Sci. Eng. B*, 2012, **177**, 705-711.

Journal of Materials Chemistry C Accepted Manuscript

30. M. Palummo, M. Amato, S. Ossicini, *Phys. Rev. B*, 2010, **82**, 073305(1-4).
31. M. Amato, M. Palummo, S. Ossicini, *Phys. Rev. B*, 2009, **80**, 235333(1-9).
32. M. Amato, M. Palummo, S. Ossicini, *Phys. Rev. B*, 2009, **79**, 201302 (R)(1-4).
33. M. Amato, M. Palummo, and S. Ossicini, *Phys. Status. Solidi B*, 2010, **247**, 2096-2101.
34. M. Amato, S. Ossicini, R. Rurali, *Nano Lett*, 2011, **11**, 594-598.
35. M. Amato, M. Palummo, S. Ossicini, *J. Comput Electron*, 2012, **11**, 272-279.
36. P. Li, R. Zhou, X. C. Zeng, *Nanoscale*, 2013, **5**, 3880-3888.
37. N. Fukata, M. Mitome, T. Sekiguchi, Y. Bando, M. Kirkham, J. Hong, Z. L. Wang, and R. L. Snyder, *ACS Nano*, 2012, **6**, 8877-8895.
38. D. C. Dillen, K. Kim, E.-S. Liu and E. Tutuc, *Nat. Nanotechnol*, 2014, **19**, 116-120.
39. D. S. Portal, P. Ordejon, E. Artacho, J. M. Soler, *Int. J. Quantum Chem.* 1997, **65**, 453-461.
40. J. P. Perdew, A. Zunger, *Phys. Rev. B*, 1981, **23**, 5048-5079.
41. E. Durgun, N. Akman, C. Ataca, and S. Ciraci, *Phys. Rev. B*, 2007, **76**, 245323.
42. H. J. Monkhorst, J. D. Pack, *Phys. Rev. B*, 1976, **13**, 5188-5192.
43. Y. Wu, Y. Cui, L. Huynh, C. J. Barrelet, D. C. Bell, C. M. Lieber, *Nano Lett.* 2004, **4**, 433-436.
44. E. Durgun, N. Akman, C. Ataca, and S. Ciraci, *Phys. Rev. B*, 2007, **76**, 245323.
45. M. Diarra, Y. M. Niquet, C. Delerue, G. Allan, *Phys. Rev. B,* 2007, **75**, 045301.

Journal of Materials Chemistry C Accepted Manuscript

Graphic abstract

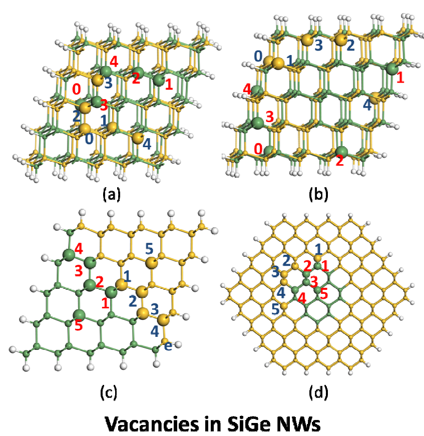

Journal of Materials Chemistry C Accepted Manuscript